12 (2022) 100252

Contents lists available at ScienceDirect

Biosensors and Bioelectronics: X

journal homepage: www.journals.elsevier.com/biosensors-and-bioelectronics-x

Enzymatic degradation of bacterial cellulose derived carbon nanofibers (BC-CNF) by myeloperoxidase (MPO): Performance evaluation for biosensing

Ruchira Nandeshwar [a], Mani Pujitha Illa [b], Mudrika Khandelwal [b,*], Siddharth Tallur [a,*]

[a] Department of Electrical Engineering, IIT Bombay, Mumbai 400076, India
[b] Department of Materials Science and Metallurgical Engineering, IIT Hyderabad, Sangareddy, Kandi 502285, Telangana, India

ARTICLE INFO

Keywords:
Myeloperoxidase
Optical sensor
Bacterial cellulose
Carbon nanofiber
Cardiovascular disease

ABSTRACT

Myeloperoxidase (MPO) is a promising biomarker for early warning of incidence of cardiovascular diseases (CVDs). Among various sensing mechanisms for detection and quantification of MPO, enzymatic degradation of carbon nanoparticles (CNPs) in presence of MPO has unique advantages such as visual change in optical contrast of sample without requiring additional probe chemicals or reagents. While the degradation of various forms of CNPs (including carbon nanotubes and graphene oxide) due to MPO has been reported in literature, the degradation is typically very slow, resulting in response times on the order of multiple hours, and thus presents a significant limitation for CVD diagnosis. Besides, the extent of degradation is highly sensitive to substrate uniformity, necessitating complicated synthesis processes to obtain pristine CNPs. In this work, we have characterized the enzymatic degradation of bacterial cellulose derived carbon nanofibers (BC-CNF) due to MPO *in vitro* and explored the feasibility of realizing a BC-CNF colorimetric biosensor for measuring MPO activity. The degradation of BC-CNFs is thoroughly characterized using SEM, TEM, Raman and UV–Vis spectroscopy. We report that carboxylic group functionalized BC-CNFs demonstrate noticeable change in optical contrast due to degradation with clinically relevant concentrations of MPO in approximately 1 h, and hold great promise for realizing low-cost biosensors for MPO.

1. Introduction

Cardiovascular diseases (CVDs) are the leading cause of deaths due to non-communicable diseases, with an estimated 17.9 million deaths in 2019, representing 32 % of all global deaths reported that year (WHO, 2022). The incidence of death due to CVDs is high in densely populated low & middle income countries (LMICs). Therefore it is essential to develop low-cost tests for better management of CVDs globally, that can be executed seamlessly without requiring highly skilled personnel. Various clinical biomarkers have been reported for diagnosis of CVDs, including C-reactive protein (CRP), B-type natriuretic peptides (BNP), N-terminal prohormone BNP (NT-proBNP), cardiac troponin I (cTnI), cardiac troponin T (cTnT) etc. Vasan (2006). The concentration of these biomarkers elevates in the bloodstream at the onset of or immediately following myocardial infarction (MCI, commonly known as heart attack). Therefore, they are useful for diagnosing heart attacks, but cannot be leveraged as early warning biomarkers for detecting vulnerability to CVDs (Vasan, 2006; Ghantous et al., 2020).

Myeloperoxidase (MPO) is an early biomarker for CVDs, that has received significant attention in recent years. MPO is stored and expressed abundantly in azurophilic granules of polymorphonuclear neutrophils and also to some extent in monocytes (Daugherty et al., 1994). Inflammation and oxidative stress contribute significantly in the pathogenesis of destabilization of coronary artery disease which leads to acute coronary syndrome (ACS) (Nicholls and Hazen, 2009; Hazen and Heinecke, 1997; Davies, 2010). MPO is a proinflammatory enzyme which acts as catalyst for oxidative modification of lipoproteins in the artery wall and can be measured in peripheral blood. MPO is present abundantly in ruptured plaque which is directly associated with ACS and atherosclerosis (Ramachandra et al., 2020). The concentration of MPO elevates in the bloodstream in advance of MCI as compared to traditional cardiac biomarkers that elevate after the heart is damaged or stressed. Various cohort studies have established MPO as an important biomarker to predict heart health (Liu et al., 2012; Sawicki et al., 2011; Kaya et al., 2012; Nicholls and Hazen, 2009). Currently all these cohort studies are performed using enzyme-linked immunosorbent assays (ELISA) kit or mass spectrometry which are highly sensitive but also expensive, require specialized reagents, skilled personnel for operating the test and long turn-around time for diagnosis (Khalilova et al., 2018). These constraints inhibit the applicability of ELISA for point-of-care diagnosis. Several sensing techniques have been reported for MPO, based on colorimetry (Bassegoda et al., 2019), chemiluminescence (Guo et al.,

* Corresponding authors.
E-mail addresses: mudrika@msme.iith.ac.in (M. Khandelwal), stallur@ee.iitb.ac.in (S. Tallur).

https://doi.org/10.1016/j.biosx.2022.100252
Received 6 April 2022; Received in revised form 12 July 2022; Accepted 8 September 2022
Available online 13 September 2022

Table 1
Summary of various studies reported in literature for enzymatic degradation of carbon nanoparticles due to MPO.

Material	Reference	Remarks/Study
SWCNT	Kagan et al. (2010)	*in vitro* degradation of IgG-SWCNT with neutrophils
	Ding et al. (2016)	*in vitro* degradation of IgG-SWCNT with and without activated neutrophils
	Vlasova et al. (2011)	Studied importance of hypochlorite in oxidative degradation of carboxylated SWCNT (c-SWCNT)
	Lu et al. (2014)	Degradation and cellular uptake of human serum albumin functionalized SWCNT (HSA-SWCNT) in neutrophils
	Bhattacharya et al. (2014)	Degradation of Poly(ethylene glycol) (PEG) functionalized SWCNT *in vitro* using recombinant myeloperoxidase and *ex vivo* using isolated primary human neutrophils
	Kotchey et al. (2013)	Effect on degradation of oxidized SWCNT (o-SWCNT) due to MPO in presence of antioxidants such as L-ascorbic acid (AA) and L-glutathione (GSH)
Graphene oxide (GO)	Kurapati et al. (2015)	Effect of dispersibility on biodegradation of GO due to human MPO (hMPO)
	Mukherjee et al. (2018)	Toxicity of products generated by degradation of GO due to MPO
	Martin et al. (2019)	Degradation of N-formyl-methionyl-leucyl-phenylalanine (fMLP) functionalized GO for targeted cancer therapy
MWCNT	Azuara-Tuexi et al. (2021)	Degradation of oxidized nitrogen doped multiwall carbon nanotubes (NMWCNT) due to hMPO
GQD	Martín et al. (2019)	Biodegradation and change in luminescence of GQDs synthesized by hydrothermal process
Fullerene C_{60}	Piotrovskiy et al. (2020)	Effect of MPO on topology and degradation of fullerene

Glossary — SWCNT: single walled carbon nanotube, MWCNT: multi walled carbon nanotube, GQD: graphene quantum dot.

2017; Zhang et al., 2013), electrochemical immunosensors (Wen et al., 2018; Bekhit and Gorski, 2019) etc. Such techniques typically require specialized processing for immobilization of antibodies on functionalized substrates and suffer loss of sensitivity when stored in ambient conditions.

MPO plays an important during the phagocytosis process, as it catalyzes chloride ions and hydrogen peroxide to form hypochlorous acid HOCl, which is a strong bactericidal agent. The generation of HOCl is related to the damage caused by oxidative stress and analyzing its levels qualitatively and quantitatively will be beneficial in determining the MPO levels. Techniques to measure HOCl mainly include use of fluorescent probes and multi-step synthesis (He et al., 2020, 2019). Production of HOCl/Cl- is an important part of human immune system. Apart from making sensors to detect HOCl, several studies have reported its role in *in vivo* and *in vitro* biodegradation of nanoparticles utilized in therapeutic, drug delivery or imaging applications (Kagan et al., 2010; Ding et al., 2016; Vlasova et al., 2011; Lu et al., 2014; Bhattacharya et al., 2014; Kotchey et al., 2013; Kurapati et al., 2015; Mukherjee et al., 2018; Martin et al., 2019; Azuara-Tuexi et al., 2021; Martín et al., 2019; Piotrovskiy et al., 2020), as summarized in Table 1.

In our previous work, we successfully demonstrated a low-cost optical phase sensitive detector (PSD) sensor to detect MPO concentration by detecting the extent of enzymatic degradation of single wall carbon nanotubes (SWCNTs) (Nandeshwar and Tallur, 2020). While this method does not utilize expensive reagents or substrates with sophisticated functionalization processes and storage requirements, there were some limitations that remained unaddressed. Synthesis of SWCNT is a complex process that adds to the manufacturing cost, and enzymatic degradation of SWCNTs due to MPO is a slow process, resulting in degradation (response) time on order of several hours (Kagan et al., 2010). In this work, we report *in vitro* biodegradation of bacterial cellulose derived carbon nanofibers (BC-CNF) due to MPO. BC-CNFs possess higher number of defects than carbon nanotubes, that facilitates faster degradation, and involve an uncomplicated synthesis process (Illa et al., 2019a). Since MPO shows higher binding affinity towards carboxyl groups in carbon nanoparticles (CNPs) (Kagan et al., 2010), we evaluated the impact of acid functionalization on structure and degradation of BC-CNFs. The key contributions of this work are as follows:

- *Acid functionalization of BC-CNFs aids enzymatic degradation*: We observed that acid functionalization leads to improved dispersibility of BC-CNFs in DI water and faster degradation as compared to SWCNT, due to MPO, with noticeable change in optical contrast observed within 1 h.
- *Proof-of-concept demonstration of CNF degradation as sensing mechanism for MPO activity detection*: We have studied the feasibility of utilizing acid functionalized BC-CNFs for colorimetric biosensing of MPO and observed that the sensor exhibits large difference in voltage output due to degradation of BC-CNFs for clinically relevant concentration of MPO ($\approx 300\,\mathrm{ng\,ml^{-1}}$).

The observations were confirmed through extensive material characterization (SEM, TEM, Raman spectroscopy, FTIR), and the change in optical contrast was validated with UV–Vis spectroscopy. To the best of our knowledge, this is the first report of enzymatic biodegradation of BC-CNFs due to MPO, and bodes well for the development of label-free, low-cost sensors for MPO. A schematic illustration of the synthesis and acid functionalization of BC-CNF and MPO induced degradation as sensing mechanism is shown in Fig. 1.

2. Materials and methods

2.1. Materials

Yeast extract, peptone, and citric acid (bacteriological grade) were procured from HiMedia Laboratories Pvt. Ltd., India. Glucose AR, di-sodium hydrogen orthophosphate dihydrate AR, sodium hydroxide (NaOH) pellets (98 %) were procured from Sisco Research Laboratories Pvt. Ltd., India. Cellulose-producing bacteria ATCC 23769 (*Komagataeibacter Hansenii*) was procured from the American Type Cell Culture society. 65–70 % nitric acid (HNO3), 95–98 % sulfuric acid (H2SO4), 98 % ethanol, IPA and phosphate buffer saline tablets (P4417), human serum (H4522) were procured from Sigma Aldrich. Hydrophilized polytetrafluoroethylene (PTFE) filter membranes (0.2 μm pore size and 47 mm diameter) were procured from Axiva Sichem Pvt. Ltd. Lyophilized human myeloperoxidase was procured from MPO Planta Natural Products, CAS No. 9003-99-0. 30 % H2O2 was procured from EMPARTA®. All dilutions were prepared in DI water, unless otherwise specified.

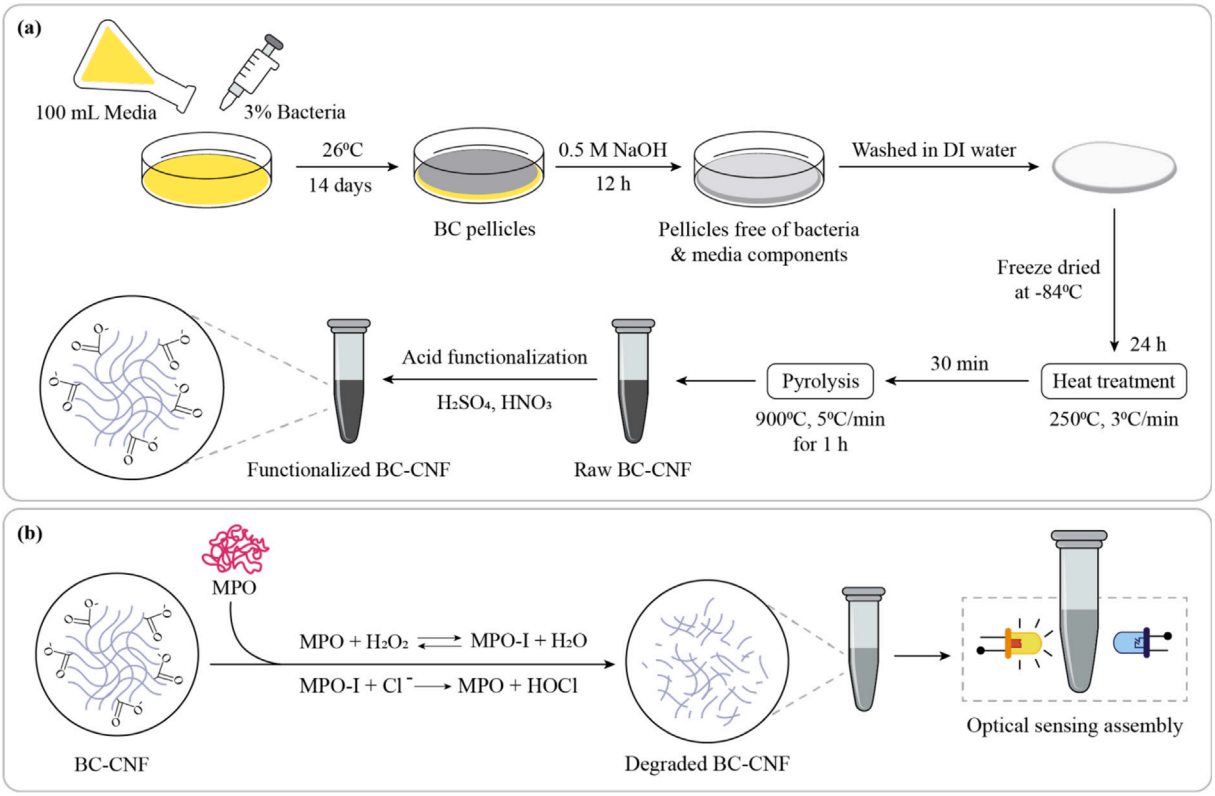

Fig. 1. (a) Schematic representation of synthesis and functionalization of BC-CNF. (b) Illustration of MPO interaction with BC-CNF and optical sensing assembly.

2.2. BC-CNF synthesis process

Bacterial cellulose (BC) synthesis process was adapted from previous work by Illa et al. (2019b). It involves inoculation and incubation of cellulose-producing bacteria in fermentation media. Hestrin Schramm (HS) media consisting of 20 g l^{-1} glucose, 5 g l^{-1} peptone, 5 g l^{-1} yeast extract, 3.4 g l^{-1} disodium orthophosphate dihydrate, and 1.15 g l^{-1} citric acid dissolved in DI water was used as fermentation media for bacterial culture. After autoclaving, 100 ml of media with 3 % inoculum of cellulose-producing bacteria (ATCC 23769) was added to 15 cm diameter petri-dishes. These inoculated petri-dishes were sealed with parafilm and incubated at 26 °C for 14 days. On the 15th day, the BC pellicles formed at the air-media interface were harvested and treated with 0.5 M NaOH solution for 12 h to remove entrapped bacteria and media components. After NaOH treatment, the treated BC pellicles were washed with DI water several times till neutral pH was achieved. The purified BC pellicles were freeze-dried at −84 °C for 24 h. The dried BC pellicles were pyrolyzed in a high-temperature tubular furnace under nitrogen atmosphere to convert them into carbon nanofibers (CNFs) (Zhang et al., 2017; Liu et al., 2015). The dried BC pellicles were first heated to 250 °C with ramp rate 3 °C min^{-1} followed by 30 min dwell time for stabilization, and then pyrolyzed at 900 °C with ramp rate 5 °C min^{-1}. The pyrolysis temperature was maintained for 1 h, before cooling down the furnace to room temperature. The synthesized BC-CNFs were stored at room temperature.

2.3. Acid functionalization of BC-CNF

To functionalize the BC-CNFs with carboxyl group, we adapted a method developed by Jun et al. for MWCNTs (Jun et al., 2018). 15 mg of raw BC-CNF (CNF-R) were dispersed in 20 ml of 15.8 M HNO3 and 60 ml of 18.4 M H2SO4. This suspension was sonicated in bath ultrasonicator at 53 kHz and 40 °C for 2.5 h. The suspension was then diluted in DI water and filtered in a vacuum filter with PTFE filter membrane. The filter cake samples were washed till neutral pH was achieved. Then the sample was dried for 12 h in an oven at 60 °C to obtain carboxylic acid-functionalized BC-CNFs (CNF-F).

2.4. Sample preparation and characterization

2.4.1. Raman spectroscopy and Fourier transform infrared spectroscopy (FTIR)

CNF-R, CNF-F, and SWCNT powders were pelletized between two glass slides. Raman spectrum of pellets thus prepared was recorded using HR800-UV confocal micro-Raman spectrometer (excitation source 532 nm, 50 mW) (Horiba Jobin Yvon, France). FTIR spectrum was recorded with 3000 Hyperion Microscope with Vertex 80 FTIR System (Bruker, Germany).

2.4.2. Scanning electron microscopy (SEM) and transmission electron microscopy (TEM)

For obtaining SEM micrographs, CNF samples were sprinkled on carbon tape, and the imaging was performed using field emission scanning electron microscope JOEL JSM-7600F (Jeol, Ltd., Japan). For TEM micrographs, the samples were drop casted onto lacey carbon grids and allowed to dry at room temperature. TEM imaging was performed with HRTEM: JEOL JEM-2100F (Jeol, Ltd., Japan) at 200 kV.

2.4.3. Study of CNF samples degraded due to MPO

Control and test samples were prepared separately to study the degradation of CNF-R and CNF-F due to MPO. Control sample for CNF-R with 310 µl volume comprised of 25 µg/ml CNF-R, 300 µM H2O2 and 9.7 mM PBS (containing 0.133 M NaCl). Test sample for CNF-R contained 310 µl total volume with final concentrations of reagents as 25 µg/ml CNF-R, 300 µM H2O2, 9.7 mM PBS and 9.67 µg/ml MPO. Note that H2O2 was added only once to the control and test samples during preparation, and not periodically thereafter unlike the method reported by Kagan et al. (2010). The test and control samples are kept under observation

for 4 h at room temperature. Similarly, test and control samples for CNF-F were prepared, keeping all parameters and concentrations same as used for CNF-R. For SEM and TEM analysis 30 μl of the sample was taken out from each test and control sample every hour and stored at −20 °C to stop any further degradation in the sample. The 0 h sample was collected before adding MPO in the test sample. At the time of sample preparation for SEM/TEM imaging, these frozen samples were first thawed and then diluted with 20 μl of DI water. The diluted samples were ultrasonicated for 5 min to disperse the sample uniformly and dropcasted on to Si wafer for SEM imaging. The wafer was cleaned using IPA, acetone and DI water. For TEM micrographs, the diluted samples were drop casted onto lacey carbon grids which were allowed to dry at room temperature. UV–Vis spectroscopy on control and test samples was performed with Lambda 25 spectrometer (PerkinElmer., USA), using 310 μl of sample in the test cuvette (polystyrene cuvette; Bio-Rad Laboratories Inc., USA), and a mixture of 300 μM H2O2 and 9.7 mM PBS as background.

2.4.4. Sample preparation for characterization with optical PSD sensor

For the characterizing enzymatic degradation of CNF-F with optical PSD sensor, test and control samples were prepared. Test sample T1 with 320 μl volume contained 50 μg/ml CNF-F, 300 μM H2O2, 9.7 mM PBS (containing 0.133 M NaCl) and 9.4 μg/ml MPO. Test sample T2 contained 306.4 ng ml^{-1} MPO, while keeping concentrations of other chemicals the same as in test sample T1. The control sample contained all chemicals except MPO. To study the sensor response for clinically relevant MPO concentrations, samples were prepared with 320 μl volume containing 30 μg/ml CNF-F, 300 μM H2O2 and 9.7 mM PBS and MPO, where the MPO concentration was varied. Lower CNF-F concentration was used as compared to samples T1 and T2, to get better resolution with lower concentrations of MPO. Sample1 S1 contained 300 ng ml^{-1} MPO, sample S2 contained 200 ng ml^{-1} MPO, sample S3 contained 100 ng ml^{-1} MPO and sample S4 contained 50 ng ml^{-1} MPO. Three test samples of each concentration were prepared to perform the experiment in triplicates. For experiments with MPO spiked in human serum, two samples with different MPO concentrations were prepared. Test serum sample TS1 with 320 μl volume contained 30 μg/ml CNF-F, 300 μM H2O2, 9.7 mM PBS (containing 0.133 M NaCl) and 1 μg/ml MPO and test sample TS2 contained 300 ng ml^{-1} MPO while keeping concentrations of other chemicals the same as in test sample TS1. The control sample contained all chemicals except MPO. Note that H2O2 was added only once to the control and test samples during preparation, and not periodically thereafter unlike the method reported by Kagan et al. (2010), Huang et al. (2021). Control and test samples were prepared in Eppendorf tubes. To record sensor response, each Eppendorf tube containing the sample was inserted in the 3D printed sample holder and the optical PSD sensor output was recorded. The Eppendorf tube was removed from the holder and inserted again to record the data, to study variability in sensor output due to manual insertion of the tube in the sample holder. Data was collected for 5 such manual re-insertions, at duration of every 30 min. Each data set comprises of 120 samples recorded over a duration of 1 min. The average of these 120 samples was calculated and considered as one data point. Therefore, 5 data points were recorded for each sample every 30 min. This experiment was performed for a total duration of 3 h.

3. Results and discussion

3.1. Effect of acid functionalization on BC-CNF dispersibility and surface properties

To check the dispersibility of acid functionalized CNF, prepared as described in Section 2.3, 2 mg of CNF-R and CNF-F were dispersed in 2 ml of DI water and ultrasonicated for 10 min and kept undisturbed for 2 h. The superior dispersibility of CNF-F as compared to CNF-R is visually noticeable, as seen in Fig. 2(a), thus indicating successful functionalization of the CNFs. The change in sample morphology was observed through SEM imaging (Figs. 2(b) and (c)). It was observed that some fibers in CNF-F were broken and appeared shorter, while the diameter of some CNF-F had increased, resulting from the introduction of defects in the CNF-F during functionalization. Similar change in diameter is reported by Park et al. during acid treatment of MWCNTs (Park et al., 2008). In comparison, the CNF-R fibers were longer and exhibited uniform diameter. We further observed that the CNF-F dispersion in water remained stable for more than 30 days, and there was no sign of CNF-F settling. The surface potential of the sample was characterized using the zeta potential (ZS XPLORER, Malvern Panalytical Ltd.). To measure zeta potential, 100 μl of 1 mg ml^{-1} of CNF-F and CNF-R samples were separately diluted in 1 ml DI water and ultrasonicated for 10 min. The zeta potential for CNF-R and CNF-F were measured to be −5.02 mV and −26.72 mV respectively. These findings confirm that CNF-F has higher magnitude of zeta potential than CNF-R, and therefore superior dispersibility.

Due to the presence of more oxygen-containing groups such as carboxyl/hydroxyl/carbonyl groups, CNF-F has higher negative charge than CNF-R. The presence of higher number of carboxyl/hydroxyl groups were further verified through FTIR spectra (Fig. 2(d)). Both CNF-R and CNF-F show a characteristic broad signature of O-H bond stretching around 3200-3700 cm^{-1}, C-H bond stretching around 2850-2920 cm^{-1} and C=C bond signature around 1650-1600 cm^{-1}, confirming that the structure of CNF is retained after functionalization (Illa et al., 2019b). The signatures around 1350 cm^{-1} and 1460 cm^{-1} are due to asymmetrical bending vibrations of CH3 and CH2 alkane bending, respectively (Cui et al., 2017). CNF-F shows additional signatures due to C=O and C-O bonds around 1665-1760 cm^{-1} and 1019-1308 cm^{-1} (Zhang et al., 2003), respectively due to the oxidation of some carbon nanofibers. This indicates successful functionalization of CNF-F. Some of these signatures were also observed for CNF-R, albeit with very low intensity.

The increase in number of defect sites in CNF-F was verified with Raman spectroscopy. Raman spectra recorded on CNF-F and CNF-R are shown in Fig. 2(e). The characteristic peaks of CNF for the *D* and *G* bands are around 1340 cm^{-1} and 1590 cm^{-1}, respectively. The *D* band is related to structural disorder and defects, whereas the *G* band corresponds to the C=C bond in the graphitic plane. An increase in I_D/I_G ratio indicates the presence of more structural defects and higher proportion of sp^3 carbon (Ngo et al., 2013). Due to the oxidation of CNF-F and the presence of carboxylic group in CNF-F, the I_D/I_G ratio is higher than I_D/I_G ratio of CNF-R (Janudin et al., 2017). The average I_D/I_G ratio based on spectra collected at three different positions for CNF-F and CNF-R were calculated to be 0.87 and 0.74, respectively.

3.2. Enzymatic degradation of BC-CNF

The degradation of several forms of CNPs in the presence of MPO summarized in Table 1 is typically a slow process that requires several hours (Kagan et al., 2010; Azuara-Tuexi et al., 2021). We have previously observed that carboxylic acid functionalized SWCNTs showed measurable degradation due to MPO over the course of 4 h (Nandeshwar and Tallur, 2020). Molecular modeling simulations reported by Kagan et al. indicate strong interaction between MPO and carboxyl groups on SWCNT surface (Kagan et al., 2010). BC-CNFs have higher defects when compared to SWCNTs (Illa et al., 2018; Zhang et al., 2003), and are expected to degrade faster. Fig. 3 shows SEM micrographs of CNF-R and CNF-F control and test samples obtained before interaction with MPO (0 h) and 2 h after interaction with MPO (for test sample). MPO was not added to the control sample. The CNF-R test sample shows fibers broken into smaller fragments after 2 h with less agglomeration. However no noticeable change in diameter was observed. The CNF-R control sample imaged after 2 h does not show any change in diameter as compared to 0 h sample. The agglomeration in the CNF-R control sample after 2 h might due to the cleavage of -OH

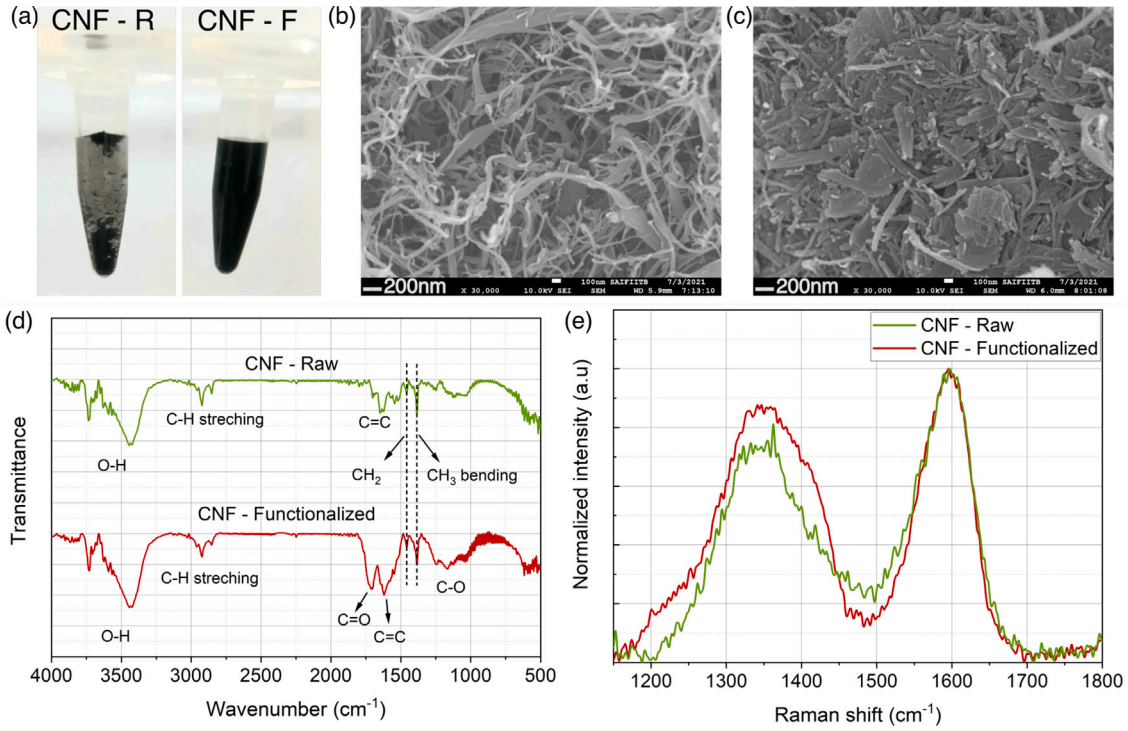

Fig. 2. (a) Photographs of raw CNF (CNF-R) and functionalized CNFs (CNF-F) dispersed in DI water and kept undisturbed for 2 h. CNF-F shows better dispersibility. (b) & (c) SEM micrographs of (b) CNF-R and (c) CNF-F, show changes in surface morphology of CNF after functionalization. (d) FTIR spectra and (e) Raman spectra of CNFs before (green, CNF-R) and after (red, CNF-F) functionalization. The Raman spectra curves are normalized to show same intensity for G band, to better visualize the increase in I_D/I_G ratio after functionalization. (For interpretation of the references to color in this figure legend, the reader is referred to the web version of this article.)

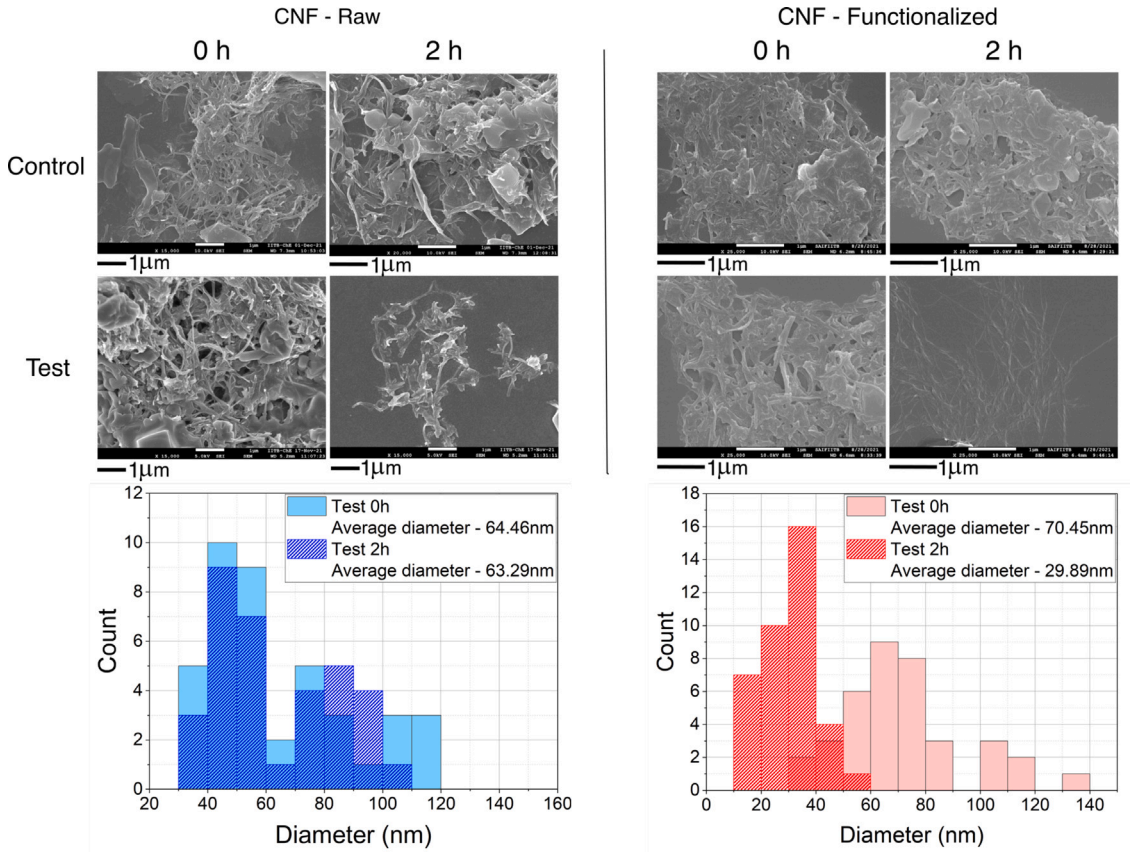

Fig. 3. SEM micrographs of CNF-R and CNF-F control and test samples taken at 0 h and 2 h after adding MPO. CNF-F shows more signs of degradation than CNF-R at 2 h. The distribution of diameter of nanofibers in CNF-F test samples shows significant change from 0 h to 2 h, while no noticeable change is noticed for CNF-R samples.

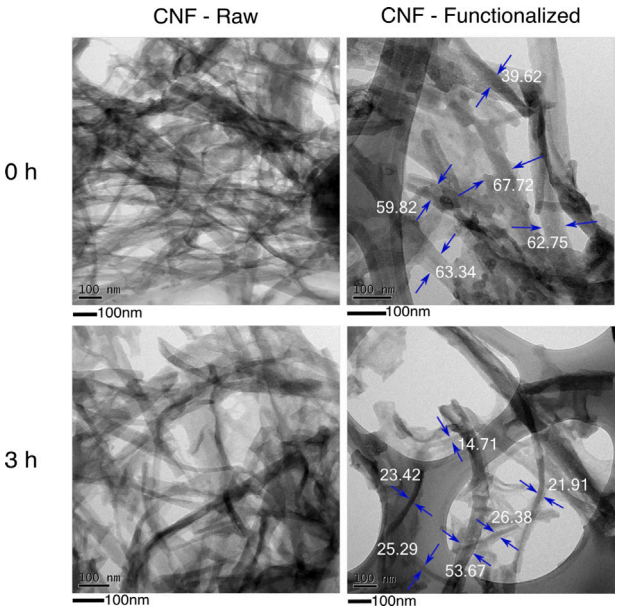

Fig. 4. TEM micrographs of CNF-R and CNF-F test samples taken at 0 h and 3 h after adding MPO. Arrows are provided as visual aids and representative diameters (nM) are indicated for CNF-F samples.

groups present on CNF-R surface by H2O2 leading to less electrostatic repulsion and more aggregation (Czech et al., 2015). In the case of the CNF-F control sample, there was no noticeable change in structure at 0 h and 2 h. However, in the CNF-F test sample imaged at 2 h, most of the smaller fragments of CNF-F were completely degraded, and only a few longer fragments remained. The average diameter of CNF-F test sample at 0 h and 2 h was measured using ImageJ software (Schneider et al., 2012) to be approximately 70.45 nm and 29.89 nm, respectively. There was no significant difference in diameter of the 0 h and 2 h test samples of CNF-R (64.46 nm and 63.29 nm, respectively). Therefore, it can be concluded that MPO plays an important role in the faster degradation of CNFs. Additional SEM images recorded every hour for CNF-F and CNF-R samples are provided in supplementary information (Figures S1 and S2, respectively). TEM results presented in Fig. 4 also support the observations made from SEM micrographs. TEM analysis was performed only for test samples of CNF-R and CNF-F, and the samples were collected for TEM imaging only at 0 h and 3 h upon adding MPO. Lesser agglomeration was observed in the CNF-F 3 h samples as compared to 0 h. The CNF-R samples show similar features at 0 h and 3 h. Compared to the 3 h image of CNF-R, the CNF-F image displays less aggregation and more degradation.

Fig. 5(a) shows photographs with visibly distinct change in test (T) CNF-F sample as compared to control (C) CNF-F sample, with increasing time. The CNF concentration used in each Eppendorf tube was 14 μg/ml. After 2 h the test sample was observed to be almost transparent while the color of the control sample had barely changed as compared to 0 h. The H2O2 and NaCl in control sample also produce hypochlorous acid that degrades the CNF, albeit far more slowly. Due to this, some settling of the partially degraded CNF-F control sample was observed after 24 h. UV–Vis spectroscopy measurements were performed with CNF-F to investigate the change in optical contrast of the functionalized CNF in presence of MPO. The samples were kept undisturbed in a polystyrene cuvette for 2 h, and the absorbance spectrum was recorded every 10 min. In Fig. 5(b), UV–Vis spectrum for CNF-F test and control samples at 0 min and 120 min are compared. While there are no characteristic peaks in the UV–Vis spectra, the absorbance curve shows drastic reduction with enzymatic degradation of CNF-F in the test sample. The UV–Vis absorbance spectrum obtained at various intermediate times are presented in supplementary information (Figure S3). Change in extent of degradation of CNF-F was studied by calculating the area under the curve (AUC) in OriginLab®, and the normalized AUC trends for control and test samples for wavelength range 800 nm-900 nm are shown in Fig. 5(c). The AUC trend in wavelength range 800 nm-900 nm is of interest for the optical PSD sensor described in the next sub-section. Change in AUC for control sample was significantly lesser as compared to test sample. The change in AUC for test sample is more pronounced after 30 min. Based on XRD analysis reported in previous work, BC-CNFs are known to possess ordered crystalline regions surrounded by amorphous carbon (Illa et al., 2019a). Reduced crystallinity as compared to SWCNTs could also explain the significantly faster degradation of CNFs observed in this work, as compared to SWCNT degradation due to MPO reported in our previous work (Nandeshwar and Tallur, 2020).

3.3. Detection of degradation of BC-CNF with optical phase sensitive detection based sensor

To explore the feasibility of utilizing enzymatic degradation of CNF-F for biosensing of MPO, we characterized the change in optical contrast due to degradation with optical PSD sensor (Nandeshwar and Tallur, 2020; Nandeshwar et al., 2018). Fig. 6(a) shows a photograph of the 3D printed package of the PSD optical sensor. Printed circuit boards (PCBs) containing the photodiode (BPW46) and infrared (IR) LED (GaAs) were inserted in the 3D printed setup as seen in the figure. The PCBs were arranged in such a way that the optical path of the LED-photodiode pair was aligned with the center of the sample holder that houses the Eppendorf tube containing the sample. The schematic of the PSD circuit is shown in Fig. 6(b). The principle of operation of this circuit is explained in detail in our previous work (Nandeshwar et al., 2018), although in this work the sample holder is redesigned for optimizing sensor performance for MPO. The circuit utilizes two arms gated by complementary control signals (labeled *Cntrl* and ~*Cntrl*), such that only one of the arms offers a connection to the difference amplifier at any time. The *Cntrl* arm is in-phase with the trigger applied to the LED, and thus the capacitor connected in the *Cntrl* arm samples the voltage generated due to light transmitted through the sample as well as ambient light. On the other hand, the capacitor connected to the ~ *Cntrl* arm samples only voltage generated due to ambient light. The difference amplifier helps in removing the contribution from the ambient light and thus improves the signal to noise ratio and

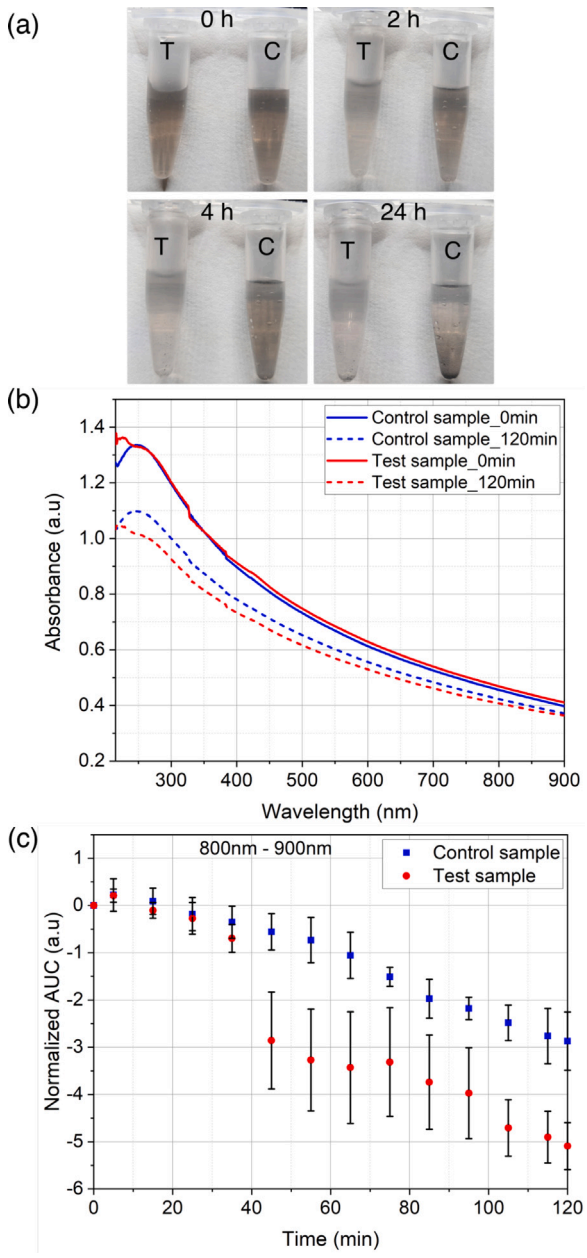

Fig. 5. (a) Change in optical contrast of CNF-F test sample (T) as compared to control sample (C) is visibly apparent, due to degradation of CNF-F after adding MPO. (b) UV–Vis spectroscopy for CNF-F test and control samples obtained at 0 min and 120 min. (c) Normalized (i.e. shift from t = 0) area under curve obtained at intervals of 10 min from UV–Vis absorbance curve for wavelength range: 800 nm-900 nm. The experiments were performed in triplicates. (For interpretation of the references to color in this figure legend, the reader is referred to the web version of this article.)

therefore, the sensitivity of the sensor. The output of the difference amplifier is recorded with a digital multimeter (Keithley DMM7510). The response curve of the sensor for various values of CNF-F concentration in DI water is shown in Fig. 6(c). Through linear regression, the sensitivity was found out to be −8.9 mV/μg/ml, with R^2 value of 0.96. The resolution (bias stability) of the sensor was determined from Allan deviation measurement to be 70.33 μV ≡ 7.9 ng ml^{-1} change in CNF-F concentration. We chose 50 μg/ml as target concentration of CNF-F for subsequent characterization, since this concentration showed significant difference in the voltage output as compared to DI water (0 μg/ml).

The variation in sensor output for test and control samples over the course of 3 h is shown in Fig. 6(d), with each box comprising of 5 measurements. The readings are normalized to show deviation from mean of the control sample at 0 h. The sensor output for the test sample increases due to MPO induced degradation, and resultant drop in contrast of the CNF-F sample. As a result, as the concentration of CNF-F drops, the voltage output rises gradually. Note that the sensor output corresponds to a weighted averaged response of the spectral sensitivity of the photodiode (relative spectral sensitivity > 0.4 in wavelength range 550-1000 nm) and peak emission wavelength range of the LED (approximately 750-900 nm). We observed a significant difference in the sensor output at 1 h for test and control samples, consistent with the UV–Vis spectroscopy results shown in Fig. 5(c). Note that a significant difference from control sample is observed for test sample T2 containing ≈ 300 ng ml^{-1} MPO, which corresponds to clinically relevant concentration of MPO (≥300 ng ml^{-1}) for individuals at risk of acute coronary syndrome and stroke Kimak et al. (2018), Baldus et al. (2003). We further characterized the sensor response with lower concentrations of MPO with samples S1, S2, S3 and S4 (prepared as described in Section 2.4.4). The variation in sensor output measured 1 h after adding MPO for these samples is shown in Fig. 7. The sensor is clearly able to distinguish between abnormal (S1: 300 ng ml^{-1}) and healthy (S2: 200 ng ml^{-1}, S3: 100 ng ml^{-1} and S4: 50 ng ml^{-1}) concentrations of MPO. This experiment was performed in triplicates. The difference in sensor output for 300 ng ml^{-1} sample in Fig. 6(d) and Fig. 7 is because lower concentration of CNF was used to determine the resolution of PSD sensor for clinically relevant concentration of MPO. The resolution for lower concentrations of MPO could be further optimized by making design improvements to increase the optical path length through the sample, and optimizing the CNF-F concentration. We observed that the sensor output for lower concentrations of MPO decreased after 0 h. This could be because of agglomeration of few CNF-Fs and settling of bigger particles at the bottom of the Eppendorf tube, where the LED and photodiode are placed. This trend is under further investigation and will be addressed in future work.

We also studied the sensor response to samples comprising of MPO spiked in human serum (samples TS1 and TS2, prepared as described in Section 2.4.4). The results of the experiment performed with these samples are presented in Figure S4 in supplementary information. No significant change in sensor response (as compared to control sample) was detected in serum samples containing MPO, and there was no visible change in contrast, even for sample TS1 containing large concentration of MPO (1 μg/ml). Human serum consists of various other constituents that can have higher affinity towards oxide/hydroxyl groups present on CNF-F surface, leading competitive inhibition with MPO. This problem could be potentially addressed by integrating the optical PSD sensor presented in this work with microfluidic chips for in situ separation of MPO from serum samples (Jebrail and Wheeler, 2009; Han et al., 2021).

4. Conclusion and future work

In summary, we have presented BC-CNF as a promising substrate for realizing MPO biosensor by leveraging change in optical contrast of BC-CNF due to MPO induced enzymatic degradation as the sensing mechanism. Preliminary results obtained with the optical PSD sensor indicate that this scheme is capable of detecting MPO activity for clinically relevant concentration of MPO (300 ng ml^{-1}). As compared to other forms of CNPs, BC-CNFs are easier and inexpensive to synthesize and functionalize, and also offer faster response time due to presence of higher number of surface defects. Evidence of functionalization was presented through Raman spectroscopy, FTIR, zeta potential and dispersibility measurements. The observations were benchmarked against SEM and TEM imaging to inspect the morphology and degraded nanostructure of the CNFs, respectively, and the change in optical properties was validated against UV–Vis spectroscopy measurements.

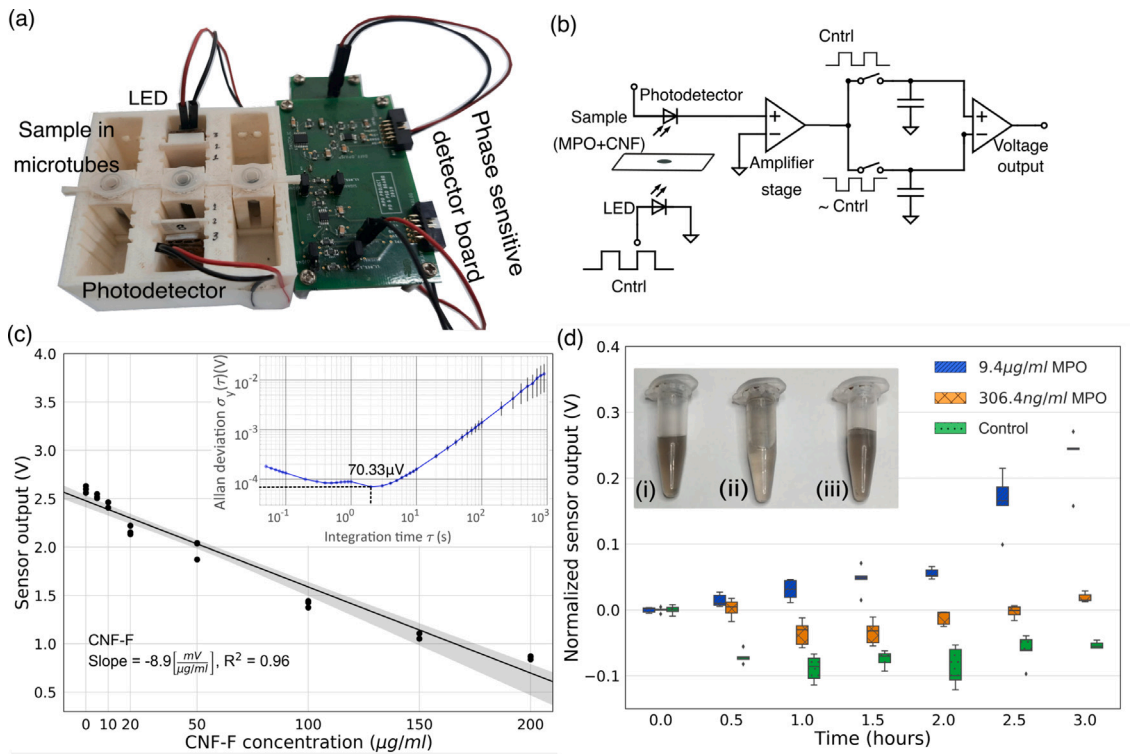

Fig. 6. (a) 3D printed setup of optical PSD sensor, showing various components. (b) Schematic diagram of the optical PSD circuit. (c) Optical PSD dose response curve for CNF-F dispersed in DI water. Inset: Allan deviation measurement for the sensor system, with measured resolution (bias stability) of 70.33 μV ≡ 7.9 ng ml^{-1} change in CNF-F concentration. (d) Normalized sensor output (i.e. shift from mean of control sample at t = 0 h) recorded every 30 min up to 3 h for CNF-F control and test samples containing two different concentrations of MPO: 9.4 μg ml^{-1} and 306.4 ng ml^{-1}. Inset: Photographs of Eppendorf tubes containing samples used for these measurements, at end of 3 h: (i) Control, (ii) 9.4 μg ml^{-1} MPO, (iii) 306.4 ng ml^{-1} MPO.

Table 2
Comparison of the BC-CNF degradation based MPO sensing technique with literature.

Reference	Substrate (sample holder)	Reagents and other materials	Auxiliary equipment
Electrochemical sensors			
Hajnsek et al. (2015)	Screen printed electrode functionalized with glucose oxidase	Glucose oxidase, PBS, glucose	Potentiostat, microfluidic pump
Bekhit and Gorski (2019)	Glassy carbon electrode, functionalized with SWCNT	SWCNT, Chitosan, antibody dipstick, NH_4SCN, PBS, H_2O_2, Pt counter wire	Electrochemistry workstation
Mondal et al. (2017)	Whatman filter paper coated with conductive polymer	Anti-MPO monoclonal antibodies, sodium phosphate buffer, glutaraldehyde, PBS	Impedance analyzer
Ruiz-Vega et al. (2017)	Lateral flow assay with paper based screen printed electrodes	streptavidin coated Magnetic beads, anti-MPO, HRP, TMB	Potentiostat
Colorimetric activity assay			
Santopolo et al. (2021)	96 well plate	Magnetic beads, Gold nanoparticles, DMSO	Plate reader, vis-NIR spectrophotometer
Abcam ab105136	96 well plate	MPO assay buffer, DNTB probe, TCEP	Microcentrifuge, colorimetric microplate reader, orbital shaker, Dounce homogenizer
Optical sensors			
Khatri et al. (2016)	Polymer waveguides with immobilized gold nanoparticles	Gold nanoparticles, anti-MPO, APTES	Spectrophotometer, LED, collimating lens, objective lens, 600 μm core optical fiber
This work	Microtubes (no functionalization)	BC-CNF, H_2O_2, PBS	None

Glossary — SWCNT: single walled carbon nanotube, PBS: phosphate buffer saline, HRP: horseradish peroxidase, DMSO: dimethyl sulfoxide.

A comparison of the resource requirements of the biosensor presented in this work with literature is presented in Table 2, to highlight the low-cost nature of our technology.

In future work, we will undertake further characterization to obtain a quantitative estimate of the MPO concentration based on the sensor output, and study methods to improve the *in vivo* degradation of BC-CNFs, while minimizing inference due to the presence of other peroxidases such as eosinophil peroxidase (EPO) and lactoperoxidase (LPO) in serum samples. Additionally, we aim to develop methods to improve the robustness and sensitivity of the optical biosensor and

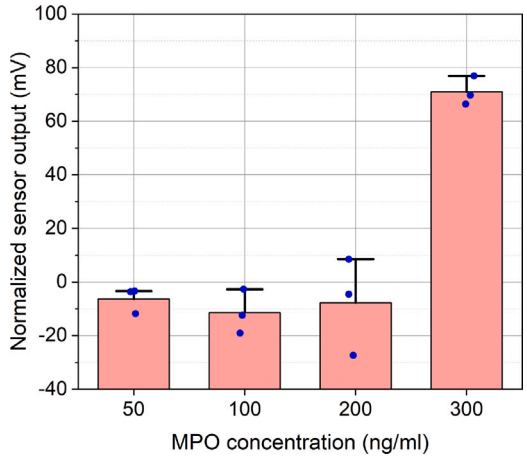

Fig. 7. Normalized sensor output (i.e. shift from mean of corresponding sample at t = 0 h) measured 1 h after introducing MPO, for samples prepared with various concentrations of MPO. The experiments were performed in triplicates.

study the impact of environmental conditions, such as temperature, pH, and ionic strength on the sensor performance. We also seek to explore the utility of other cost effective cellulose CNF for such biosensors, such as plant based nano-cellulose CNF. We also aim to improve the packaging of the optical sensor through microfluidics based designs for introducing the sample into the optical path, to avoid risk of infection and variability in sensor output due to manual handling of samples. With further development, the platform presented in this work could be utilized for low-cost point-of-use biosensor for better management of CVDs in LMICs.

CRediT authorship contribution statement

Ruchira Nandeshwar: Conceptualization, Investigation, Formal analysis, Methodology, Writing – original draft. **Mani Pujitha Illa:** Methodology, Validation, Writing – review & editing. **Mudrika Khandelwal:** Conceptualization, Funding acquisition, Resources, Writing – review & editing. **Siddharth Tallur:** Conceptualization, Funding acquisition, Resources, Writing – review & editing.

Declaration of competing interest

The authors declare that they have no known competing financial interests or personal relationships that could have appeared to influence the work reported in this paper.

Acknowledgments

R.N. acknowledges Ministry of Education (formerly Ministry of Human Resource Development), Government of India, for supporting her Ph.D. scholarship. The authors thank Ms. Rutuja Chalke at IIT Bombay for help with preparing Fig. 1. This work was supported in part by a grant from Wadhwani Research Centre for Bioengineering (WRCB) at IIT Bombay, India [grant DO/2018-WRCB002-050 awarded to S.T.]. Research in M.K. lab was supported in part through CSR grant by AT&T Inc., India

Appendix A. Supplementary data

Supplementary material related to this article can be found online at https://doi.org/10.1016/j.biosx.2022.100252.

References

Azuara-Tuexi, G., Méndez-Cabañas, J., Muñoz-Sandoval, E., Guirado-López, R., 2021. Myeloperoxidase-induced degradation of N-doped carbon nanotubes: Revealing possible atomistic mechanisms underlying hypochlorite-driven damage of nanotube walls. Carbon 175, 387–402.

Baldus, S., Heeschen, C., Meinertz, T., Zeiher, A.M., Eiserich, J.P., Münzel, T., Simoons, M.L., Hamm, C.W., 2003. Myeloperoxidase serum levels predict risk in patients with acute coronary syndromes. Circulation 108 (12), 1440–1445.

Bassegoda, A., Ferreres, G., Pérez-Rafael, S., Hinojosa-Caballero, D., Torrent-Burgués, J., Tzanov, T., 2019. New myeloperoxidase detection system based on enzyme-catalysed oxidative synthesis of a dye for paper-based diagnostic devices. Talanta 194, 469–474.

Bekhit, M., Gorski, W., 2019. Electrochemical assays and immunoassays of the myeloperoxidase/SCN–/H2O2 system. Anal. Chem. 91 (4), 3163–3169.

Bhattacharya, K., Sacchetti, C., El-Sayed, R., Fornara, A., Kotchey, G.P., Gaugler, J.A., Star, A., Bottini, M., Fadeel, B., 2014. Enzymatic 'stripping'and degradation of pegylated carbon nanotubes. Nanoscale 6 (24), 14686–14690.

Cui, H., Yan, X., Monasterio, M., Xing, F., 2017. Effects of various surfactants on the dispersion of MWCNTs–OH in aqueous solution. Nanomaterials 7 (9), 262.

Czech, B., Oleszczuk, P., Wiącek, A., 2015. Advanced oxidation (H2O2 and/or UV) of functionalized carbon nanotubes (CNT-OH and CNT-COOH) and its influence on the stabilization of CNTs in water and tannic acid solution. Environ. Pollut. 200, 161–167.

Daugherty, A., Dunn, J.L., Rateri, D.L., Heinecke, J.W., 1994. Myeloperoxidase, a catalyst for lipoprotein oxidation, is expressed in human atherosclerotic lesions. J. Clin. Invest. 94 (1), 437–444.

Davies, M.J., 2010. Myeloperoxidase-derived oxidation: mechanisms of biological damage and its prevention. J. Clin. Biochem. Nutr. 48 (1), 8–19.

Ding, Y., Tian, R., Yang, Z., Chen, J., Lu, N., 2016. Binding of human IgG to single-walled carbon nanotubes accelerated myeloperoxidase-mediated degradation in activated neutrophils. Biophys. Chem. 218, 36–41.

Ghantous, C.M., Kamareddine, L., Farhat, R., Zouein, F.A., Mondello, S., Kobeissy, F., Zeidan, A., 2020. Advances in cardiovascular biomarker discovery. Biomedicines 8 (12), 552.

Guo, J., Tao, H., Dou, Y., Li, L., Xu, X., Zhang, Q., Cheng, J., Han, S., Huang, J., Li, X., Li, X., Zhang, J., 2017. A myeloperoxidase-responsive and biodegradable luminescent material for real-time imaging of inflammatory diseases. Mater. Today 20 (9), 493–500.

Hajnsek, M., Schiffer, D., Harrich, D., Koller, D., Verient, V., vd Palen, J., Heinzle, A., Binder, B., Sigl, E., Sinner, F., et al., 2015. An electrochemical sensor for fast detection of wound infection based on myeloperoxidase activity. Sensors Actuators B 209, 265–274.

Han, Z., Peng, C., Yi, J., Zhang, D., Xiang, X., Peng, X., Su, B., Liu, B., Shen, Y., Qiao, L., 2021. Highly efficient exosome purification from human plasma by tangential flow filtration based microfluidic chip. Sensors Actuators B 333, 129563.

Hazen, S.L., Heinecke, J.W., 1997. 3-Chlorotyrosine, a specific marker of myeloperoxidase-catalyzed oxidation, is markedly elevated in low density lipoprotein isolated from human atherosclerotic intima. J. Clin. Invest. 99 (9), 2075–2081.

He, X., Chen, H., Xu, C., Fan, J., Xu, W., Li, Y., Deng, H., Shen, J., 2020. Ratiometric and colorimetric fluorescent probe for hypochlorite monitor and application for bioimaging in living cells, bacteria and zebrafish. J. Hard Mater. 388, 122029.

He, X., Wu, C., Qian, Y., Li, Y., Ding, F., Zhou, Z., Shen, J., 2019. Symmetrical bis-salophen probe serves as a selectively and sensitively fluorescent switch of gallium ions in living cells and zebrafish. Talanta 205, 120118.

Huang, S., Li, S., Liu, Y., Ghalandari, B., Hao, L., Huang, C., Su, W., Ke, Y., Cui, D., Zhi, X., et al., 2021. Neutrophils defensively degrade graphene oxide in a lateral dimension dependent manner through two distinct myeloperoxidase mediated mechanisms.

Illa, M.P., Khandelwal, M., Sharma, C.S., 2018. Bacterial cellulose-derived carbon nanofibers as anode for lithium-ion batteries. Emergent Mater. 1 (3), 105–120.

Illa, M.P., Khandelwal, M., Sharma, C.S., 2019a. Modulated dehydration for enhanced anodic performance of bacterial cellulose derived carbon nanofibers. ChemistrySelect 4 (21), 6642–6650.

Illa, M.P., Sharma, C.S., Khandelwal, M., 2019b. Tuning the physiochemical properties of bacterial cellulose: Effect of drying conditions. J. Mater. Sci. 54 (18), 12024–12035.

Janudin, N., Abdullah, L.C., Abdullah, N., Md Yasin, F., Saidi, N.M., Kasim, N.A.M., 2017. Comparison and characterization of acid functionalization of multi walled carbon nanotubes using various methods. Solid State Phenomena 264, 83–86.

Jebrail, M.J., Wheeler, A.R., 2009. Digital microfluidic method for protein extraction by precipitation. Anal. Chem. 81 (1), 330–335.

Jun, L.Y., Mubarak, N., Yon, L.S., Bing, C.H., Khalid, M., Abdullah, E., 2018. Comparative study of acid functionalization of carbon nanotube via ultrasonic and reflux mechanism. J. Environ. Chem. Eng. 6 (5), 5889–5896.

Kagan, V.E., Konduru, N.V., Feng, W., Allen, B.L., Conroy, J., Volkov, Y., Vlasova, I.I., Belikova, N.A., Yanamala, N., Kapralov, A., Tyurina, Y.Y., Shi, J., Kisin, E.R., Murray, A.R., Franks, J., Stolz, D., Gou, P., Klein-Seetharaman, J., Fadeel, B., Star, A., Shvedova, A.A., 2010. Carbon nanotubes degraded by neutrophil myeloperoxidase induce less pulmonary inflammation. Nature Nanotechnol. 5 (5), 354–359.

Kaya, M.G., Yalcin, R., Okyay, K., Poyraz, F., Bayraktar, N., Pasaoglu, H., Boyaci, B., Cengel, A., 2012. Potential role of plasma myeloperoxidase level in predicting long-term outcome of acute myocardial infarction. Tex. Heart. Inst. J. 39 (4), 500.

Khalilova, I.S., Dickerhof, N., Mocatta, T.J., Bhagra, C.J., McClean, D.R., Obinger, C., Kettle, A.J., 2018. A myeloperoxidase precursor, pro-myeloperoxidase, is present in human plasma and elevated in cardiovascular disease patients. PLoS One 13 (3), e0192952.

Khatri, A., Punjabi, N., Dhawangale, A., Mukherji, S., 2016. Inexpensive polyester sheet based waveguides for detection of cardiac biomarker, myeloperoxidase. Procedia Eng. 168, 125–128.

Kimak, E., Zieba, B., Duma, D., Solski, J., 2018. Myeloperoxidase level and inflammatory markers and lipid and lipoprotein parameters in stable coronary artery disease. Lipids Health Dis. 17 (1), 1–7.

Kotchey, G.P., Gaugler, J.A., Kapralov, A.A., Kagan, V.E., Star, A., 2013. Effect of antioxidants on enzyme-catalysed biodegradation of carbon nanotubes. J. Mater. Chem. B 1 (3), 302–309.

Kurapati, R., Russier, J., Squillaci, M.A., Treossi, E., Ménard-Moyon, C., Del Rio-Castillo, A.E., Vazquez, E., Samorì, P., Palermo, V., Bianco, A., 2015. Dispersibility-dependent biodegradation of graphene oxide by myeloperoxidase. Small 11 (32), 3985–3994.

Liu, Y., Lu, T., Sun, Z., Chua, D.H., Pan, L., 2015. Ultra-thin carbon nanofiber networks derived from bacterial cellulose for capacitive deionization. J. Mater. Chem. A 3 (16), 8693–8700.

Liu, C., Xie, G., Huang, W., Yang, Y., Li, P., Tu, Z., 2012. Elevated serum myeloperoxidase activities are significantly associated with the prevalence of ACS and high LDL-C levels in CHD patients. J. Atheroscler. Thromb. 1201100462.

Lu, N., Li, J., Tian, R., Peng, Y.-Y., 2014. Binding of human serum albumin to single-walled carbon nanotubes activated neutrophils to increase production of hypochlorous acid, the oxidant capable of degrading nanotubes. Chem. Res. Toxicol. 27 (6), 1070–1077.

Martín, C., Jun, G., Schurhammer, R., Reina, G., Chen, P., Bianco, A., Ménard-Moyon, C., 2019. Enzymatic degradation of graphene quantum dots by human peroxidases. Small 15 (52), 1905405.

Martin, C., Ruiz, A., Keshavan, S., Reina, G., Murera, D., Nishina, Y., Fadeel, B., Bianco, A., 2019. A biodegradable multifunctional graphene oxide platform for targeted cancer therapy. Adv. Funct. Mater. 29 (39), 1901761.

Mondal, D., Paul, D., Mukherji, S., 2017. Impedance spectroscopy-based detection of cardiac biomarkers on polyaniline coated filter paper. IEEE Sens. J. 17 (16), 5021–5029.

Mukherjee, S.P., Gliga, A.R., Lazzaretto, B., Brandner, B., Fielden, M., Vogt, C., Newman, L., Rodrigues, A.F., Shao, W., Fournier, P.M., et al., 2018. Graphene oxide is degraded by neutrophils and the degradation products are non-genotoxic. Nanoscale 10 (3), 1180–1188.

Nandeshwar, R., Maheshwari, N., Tallur, S., 2018. Precision low cost phase sensitive optical sensor for detecting carbon nanoparticle degradation. In: 2018 IEEE SENSORS. IEEE, pp. 1–3.

Nandeshwar, R., Tallur, S., 2020. Integrated low cost optical biosensor for high resolution sensing of myeloperoxidase (MPO) activity through carbon nanotube degradation. IEEE Sens. J. 21 (2), 1236–1243.

Ngo, C.L., Le, Q.T., Ngo, T.T., Nguyen, D.N., Vu, M.T., 2013. Surface modification and functionalization of carbon nanotube with some organic compounds. Adv. Nat. Sci.: Nanosci. Nanotechnol. 4 (3), 035017.

Nicholls, S.J., Hazen, S.L., 2009. Myeloperoxidase, modified lipoproteins, and atherogenesis. J. Lipid Res. 50, S346–S351.

Park, H.J., Park, M., Chang, J.Y., Lee, H., 2008. The effect of pre-treatment methods on morphology and size distribution of multi-walled carbon nanotubes. Nanotechnology 19 (33), 335702.

Piotrovskiy, L.B., Litasova, E.V., Sokolov, A.V., Iljin, V.V., Utsal, V.A., Zhurkovich, I.K., 2020. Degradation of fullerene C60 by human myeloperoxidase and some reaction products. Fullerenes Nanotubes Carbon Nanostruct. 28 (3), 196–201.

Ramachandra, C.J., Ja, K.M.M., Chua, J., Cong, S., Shim, W., Hausenloy, D.J., 2020. Myeloperoxidase as a multifaceted target for cardiovascular protection. Antioxid. Redox Signal. 32 (15), 1135–1149.

Ruiz-Vega, G., Kitsara, M., Pellitero, M.A., Baldrich, E., del Campo, F.J., 2017. Electrochemical lateral flow devices: Towards rapid immunomagnetic assays. ChemElectroChem 4 (4), 880–889.

Santopolo, G., Clemente, A., Aranda, M., Socias, A., Del Castillo, A., Chica, A., Borges, M., de la Rica, R., 2021. Colorimetric detection of sepsis-derived hyperdegranulation with plasmonic nanosensors. ACS Sensors 6 (12), 4443–4450.

Sawicki, M., Sypniewska, G., Kozinski, M., Gruszka, M., Krintus, M., Obonska, K., Pilaczynska-Cemel, M., Kubica, J., 2011. Diagnostic efficacy of myeloperoxidase for the detection of acute coronary syndromes. Eur. J. Clin. Invest. 41 (6), 667–671.

Schneider, C.A., Rasband, W.S., Eliceiri, K.W., 2012. NIH image to ImageJ: 25 years of image analysis. Nature Methods 9 (7), 671–675.

Vasan, R.S., 2006. Biomarkers of cardiovascular disease: Molecular basis and practical considerations. Circulation 113 (19), 2335–2362.

Vlasova, I., Vakhrusheva, T., Sokolov, A., Kostevich, V., Ragimov, A., 2011. Peroxidase-induced degradation of single-walled carbon nanotubes: Hypochlorite is a major oxidant capable of in vivo degradation of carbon nanotubes. J. Phys.: Conf. Ser. 291 (1), 012056.

Wen, Y., Yuan, J., Chen, J., Zhao, Y., Niu, Y., Yu, C., 2018. Amperometric myeloperoxidase immunoassay based on the use of CuPdPt nanowire networks. Microchim. Acta 185 (1), 1–8.

WHO, 2022. WHO cardiovascular diseases (CVDs) fact sheet. Available [Online]: https://www.who.int/news-room/fact-sheets/detail/cardiovascular-diseases-(cvds).

Zhang, T., Chen, J., Yang, B., Li, H., Lei, S., Ding, X., 2017. Enhanced capacities of carbon nanosheets derived from functionalized bacterial cellulose as anodes for sodium ion batteries. RSC Adv. 7 (79), 50336–50342.

Zhang, N., Francis, K.P., Prakash, A., Ansaldi, D., 2013. Enhanced detection of myeloperoxidase activity in deep tissues through luminescent excitation of near-infrared nanoparticles. Nat. Med. 19 (4), 500–505.

Zhang, J., Zou, H., Qing, Q., Yang, Y., Li, Q., Liu, Z., Guo, X., Du, Z., 2003. Effect of chemical oxidation on the structure of single-walled carbon nanotubes. J. Phys. Chem. B 107 (16), 3712–3718.